VIII International Conference on Fracture Mechanics of Concrete and Concrete Structures
FraMCoS-8
J.G.M. Van Mier, G. Ruiz, C. Andrade, R.C. Yu and X.X. Zhang (Eds)

A FINITE ELEMENT APPROACH FOR PREDICTING THE ULTIMATE ROTATION CAPACITY OF RC BEAMS

Eduardo A. Rodrigues[†], Osvaldo L. Manzoli[‡], Túlio N. Bittencourt[†]*, Luís A. G. Bitencourt Jr.[†] and Plínio G. C. dos Prazeres[†]

[†]Polytechnic School at the University of São Paulo (EPUSP)
Department of Structural and Geotechnical Engineering, São Paulo-SP, Brazil
e-mail: eduardoalex@usp.br - web page: http://www.usp.br

[‡] State University of São Paulo (unesp)
department of civil engineering, bauru-sp, brazil
e-mail: omanzoli@feb.unesp.br - web page: http://www.feb.unesp.br

Key words: Damage model, nonlinear analysis, Rotation capacity, Size-scale effects, Reinforced concrete.

Abstract: This paper presents a numerical approach to model the complex failure mechanisms that define the ultimate rotational capacity of reinforced concrete beams. The behavior in tension and compression is described by a constitutive damage model derived from a combination of two specific damage models [1]. The nonlinear behavior of the compressed region is treated by the compressive damage model based on the Drucker-Prager criterion written in terms of the effective stresses. The tensile damage model employs a failure criterion based on the strain energy associated with the positive part the effective stress tensor. This model is used to describe the behavior of very thin bands of strain localization, which are embedded in finite elements to represent multiple cracks that occur in the tensioned region [2]. The softening law establishes dissipation energy compatible with the fracture energy of the concrete. The reinforcing steel bars are modeled by truss elements with elastic-perfect plastic behavior.
It is shown that the resulting approach is able to predict the different stages of the collapse mechanism of beams with distinct sizes and reinforcement ratios. The tensile damage model and the finite element embedded crack approach are able to describe the stiffness reduction due to concrete cracking in the tensile zone. The truss elements are able to reproduce the effects of steel yielding and, finally, the compressive damage model is able to describe the non-linear behavior of the compressive zone until the complete collapse of the beam due to crushing of concrete. The proposed approach is able to predict well the plastic rotation capacity of tested beams [3], including size-scale effects.

1 INTRODUCTION

The development of ductility is influenced by several parameters, which makes it difficult to create a predictive model that can fully describe the mechanical behavior of reinforced concrete (RC) beams. Increasing their ductility provides a greater margin of safety because it favors greater dissipation of energy during the process that precedes collapse. Thus, in structural design, it is extremely important to analyze plastic rotation capacity, seeking mainly to know and simulate as accurately as possible the nonlinear behavior of concrete in the compressed region.

Aiming to represent nonlinear behavior, especially in compression, Carpinteri et al. [4,5] proposed a numerical model that represents the plastic rotation capacity of RC beams subjected to bending. The model is based on the concept of localization of deformation, which is able to represent the

crack growth and the crushing of concrete in the loading process. To represent the nonlinear behavior in compression, the compressed region is described according to the overlapping crack model, which describes the localization of deformation due to crushing failure by interpenetration of the material. Thus, the cohesive crack model is proposed to represent the behavior of concrete under tension and compression. The process of fracturing and crushing failure is completely localized in the central cross section representative of concrete in flexure. The stress-strain behavior in the central cross section is linear-elastic until the ultimate strength of the concrete is reached. The stresses in the cohesive zone are thus governed by functions that describe their evolution with the relative displacement of opening or interpenetration, returning a null value when the displacement reaches a critical value [4,5].

This work aimed to create a more general computational model to describe the nonlinear behavior and its influence on the ductility of reinforced concrete structures. The behavior of tensioned and compressed concrete is described by models based on Continuum Damage Mechanics [6], which has been used as an important tool to represent the state of degradation of quasi-brittle materials due to its relative simplicity, versatility and consistency [7].

The combined damage model proposed by [1] is used here to model the crack process in the tensioned region and crushing failure in the compressed region. The effect of crack formation is modeled using finite elements with embedded cracks, within the context of the Continuum Strong Discontinuity Approach (CSDA) [2,8-14], which has been applied successfully to cases in which structural nonlinearity arises predominantly from states of tension. To represent the nonlinear behavior of compression, we use an approximation of distributed cracks and a Drucker-Prager degradation criterion based on the effective stresses.

The models are composed in series, applying first the compressive damage model, using purely elastic stresses as effective stresses. The stresses degraded by the compressive damage model are then treated as effective stress by the tensile damage model [1].

The experimental tests reported by [3] were simulated numerically, seeking to predict the plastic rotation capacity of RC beams. The tension and compression reinforcement rate, as well as the beams' dimensions, were varied in order to reproduce the size-scale effect evidenced in the experimental results.

2 NUMERICAL FORMULATION

The methodology used in this paper to describe the aforementioned numerical simulation of plastic rotation capacity is organized as follows:

- ✓ First, we present the mathematical formulation for the compressive damage model. The model is formulated in the effective stress field, based on the Drucker-Prager criterion, which was originally formulated in 1952 and resulted from the modification of the von Mises criterion so as to include the effect of hydrostatic pressure.
- ✓ The tensile damage model is then described, whose degradation criterion is based on the strain energy of the positive part of the effective stress tensor [15,16]. The model is able to represent the formation of discontinuities in the displacement field in quasi-brittle materials.
- ✓ An explanation is then given on the composition of the two models in series proposed by [1], where the strain degraded by the compressive damage model is treated as effective stress by the tensile damage model. This model, based solely on continuum damage mechanics, is able to represent the behavior of materials that exhibit different responses when subjected to tensile or compressive loads. The combined model can also deal with alternating loads (tension and compression), involving closing and reopening of existing cracks.
- ✓ Lastly, a brief description is given of the formulation of finite elements with embedded cracks in the context of the

Continuum Strong Discontinuity Approach (CSDA) [2,11].

2.1 Compressive damage model

The effective stress tensor can be divided into a volumetric and a deviatoric part, as follows:

$$\overline{\boldsymbol{\sigma}} = \overline{\mathbf{S}} + \overline{\sigma}_m \cdot \mathbf{I} = \overline{\mathbf{S}} + \overline{\mathbf{P}} \tag{1}$$

where $\overline{\mathbf{S}}$ is the deviatoric stress tensor, $\overline{\sigma}_m$ is the mean stress and $\mathbf{I}$ is the second-order identity tensor and $\overline{\mathbf{P}} = \overline{\sigma}_m \cdot \mathbf{I}$ is the volumetric stress tensor.

When applying the damage variable, d, only to degrade the deviatoric stress tensor, the expression of the nominal stress tensor is given by:

$$\boldsymbol{\sigma} = (1-d)\overline{\mathbf{S}} + \overline{\sigma}_m \cdot \mathbf{I}$$

which can also be expressed as:

$$\boldsymbol{\sigma} = \overline{\boldsymbol{\sigma}} - d \cdot \overline{\mathbf{S}} \tag{2}$$

Note that the deviatoric and volumetric parts of the nominal stresses are given, respectively, by $\mathbf{S} = (1-d)\overline{\mathbf{S}}$ and $\mathbf{P} = \overline{\mathbf{P}}$.

The damage criterion can be expressed in the effective stress field as:

$$F(\tau, r) = \tau(\overline{\boldsymbol{\sigma}}) - \overline{r} \leq 0 \tag{3}$$

where the scalar variable τ is defined as:

$$\tau(\overline{\boldsymbol{\sigma}}) = \|\overline{\mathbf{S}}\| + \alpha\overline{\sigma}_m \tag{4}$$

and $\overline{r}$ is the internal variable of the strain type, which establish the size of the elastic domain in the effective stress field.

In the nominal stress field, the damage criterion can be written by multiplying the two members of Eq. (3) by $(1-d)$,

$$\tau(\boldsymbol{\sigma}) = \|\mathbf{S}\| + \alpha\overline{\sigma}_m = (1-d)\overline{r} + d\alpha\overline{\sigma}_m = q(\overline{r}) \tag{5}$$

Based on Eq. (5), the damage variable can be written in terms of the internal variable of the stress type, $q(\overline{r})$, which defines a hardening/softening law:

$$d = \frac{q(\overline{r}) - \overline{r}}{\alpha\overline{\sigma}_m - \overline{r}} \tag{6}$$

An initial value is defined for the damage threshold, r_0, as a function of the ultimate compressive stress, σ_c:

$$r_0 = \left(\sqrt{\frac{2}{3}} - \frac{\alpha}{3}\right)|\sigma_c| \tag{7}$$

The evolution of the damage threshold can be expressed in closed form, always using the highest value reached by τ during the loading process, i.e., $r = \max(r, \tau)$.

The evolution of the damage variable can be defined by establishing a linear hardening law:

$$q(r) = H(r - r_0) + r_0 \tag{8}$$

where H is the linear hardening parameter.

2.2 Tensile damage model

In this case, the effective stress tensor is decomposed into positive and negative parts (positive and negative components of the effective stress tensor, respectively),

$$\overline{\boldsymbol{\sigma}}^t = \overline{\boldsymbol{\sigma}}^+ + \overline{\boldsymbol{\sigma}}^- \tag{9}$$

where $\overline{\boldsymbol{\sigma}}^+$ and $\overline{\boldsymbol{\sigma}}^-$ are effective stress tensors containing, respectively, the principal tensile and compressive stresses:

$$\overline{\boldsymbol{\sigma}}^+ = \langle\overline{\boldsymbol{\sigma}}\rangle = \sum_{i=1}^{3}\langle\overline{\sigma}_i\rangle\mathbf{p}_\mathbf{i} \otimes \mathbf{p}_\mathbf{i} \tag{10}$$

where $\overline{\sigma}_i$ denotes the value of the *i-th* principal stress of tensor $\overline{\boldsymbol{\sigma}}$, $\mathbf{p}_\mathbf{i}$ represents the unitary vector associated with the respective principal direction, and the symbol $\otimes$ denotes the tensor product. The symbol $\langle\cdot\rangle$ represents the Macaulay function (returning the value of the expression when positive, and zero otherwise).

The negative component of the effective stress tensor can be obtained as follows:

$$\overline{\boldsymbol{\sigma}}^- = \overline{\boldsymbol{\sigma}} - \overline{\boldsymbol{\sigma}}^+ \tag{11}$$

To establish the loading, unloading and reloading conditions, the damage criterion is defined by using the concept of effective tensile stress,

$$F^t\left(\bar{\tau}^t, r^t\right) = \bar{\tau}^t\left(\bar{\boldsymbol{\sigma}}^+\right) - r^t \leq 0 \qquad (12)$$

where $\bar{\tau}^t$ returns a scalar value as a function of the positive component of the effective stresses. The variable r^t establishes the damage threshold, controlling the size of the elastic domain in the space of the effective stresses. The damage threshold is bound by the surface $F^t\left(\tau^t, r^t\right) = 0$.

The standard energy tensor is adopted:

$$\bar{\tau}^t = \sqrt{\bar{\boldsymbol{\sigma}}^+ : \mathbf{C}^{-1} : \bar{\boldsymbol{\sigma}}^+} = \bar{\tau}^t\left(\bar{\boldsymbol{\sigma}}^+\right) \qquad (13)$$

where $\mathbf{C}$ is the constitutive fourth-order isotropic elasticity tensor.

The initial value of the damage threshold is expressed in terms of tensile strength, σ_t,

$$r_0^t = \frac{\sigma_t}{\sqrt{E}} \qquad (14)$$

The evolution of the tensile damage variable is defined as a function of the damage threshold variable,

$$d^t\left(r^t\right) = 1 - \frac{r_0^t}{r^t} e^{A\left(1 - \frac{r^t}{r_0^t}\right)} \qquad (15)$$

which establishes an exponential softening law, in terms of the exponential softening parameter, A.

Therefore, the constitutive law can finally be expressed as:

$$\boldsymbol{\sigma}^{\mathbf{t}} = \left(1 - d^t\right)\bar{\boldsymbol{\sigma}}^+ + \bar{\boldsymbol{\sigma}}^-$$

or

$$\boldsymbol{\sigma}^{\mathbf{t}} = \bar{\boldsymbol{\sigma}} - d^t \cdot \bar{\boldsymbol{\sigma}}^+ \qquad (16)$$

2.3 Combined damage model

The models are composed in series, first applying the compressive damage model, using as effective stresses the purely elastic stresses, calculated from the strains, $\boldsymbol{\varepsilon}$,

$$\bar{\boldsymbol{\sigma}} = \mathbf{C} : \boldsymbol{\varepsilon} \qquad (17)$$

The tensile damage model is then applied, admitting that the effective stresses for this model are the stresses degraded by the application of the compressive damage model, i.e.,

$$\bar{\boldsymbol{\sigma}}^{\boldsymbol{t}} = \boldsymbol{\sigma} \qquad (18)$$

Thus, the constitutive law for the combined model can be expressed as follows:

$$\boldsymbol{\sigma} = \Sigma^t\left(\Sigma\left(\bar{\boldsymbol{\sigma}}\right)\right) \qquad (19)$$

where Σ and Σ^t represent the constitutive relationships of the compressive and tensile damage models, respectively.

2.4 Two-dimensional finite element with embedded localization band

The effect of crack formation is modeled using finite elements with embedded cracks, within the context of the Continuum Strong Discontinuity Approach – CSDA.

Figure 1 illustrates the finite element with a strain localization band, S_e, where the formulation of the finite element with embedded crack starts from the imposition of a jump in the displacement field, $[\![\mathbf{u}]\!]$, producing a relative movement of rigid body in the continuum region, Ω_e, [2].

To represent the tensile fracture process, the nonlinear behavior in the region of strain localization (fracture process zone) is described according to the combined damage model, Σ^C, with the exponential stress softening law. The continuum region is described according to the compressive damage model, Σ, based on the nonlinear behavior in compression. The surface forces in the region of strain localization must be in equilibrium with the calculated forces in the proximities (points in the continuum region bordering the strain localization region), i.e., the vector space of stresses should have:

$$\mathbf{F}([\![\mathbf{u}]\!]) = 0$$

$$\mathbf{N}^T\left(\boldsymbol{\Sigma}^C\left(\hat{\boldsymbol{\varepsilon}} + \left(\frac{\mathbf{N}}{k} - \frac{\mathbf{M}}{l_e}\right)[\![\mathbf{u}]\!]\right) - \boldsymbol{\Sigma}\left(\hat{\boldsymbol{\varepsilon}} - \frac{\mathbf{M}}{l_e}[\![\mathbf{u}]\!]\right)\right) = 0 \qquad (20)$$

The jump $[[\mathbf{u}]]$ in the element can be obtained by solving Eq. (20) for a given strain state by means of the Newton-Raphson iterative method [1].

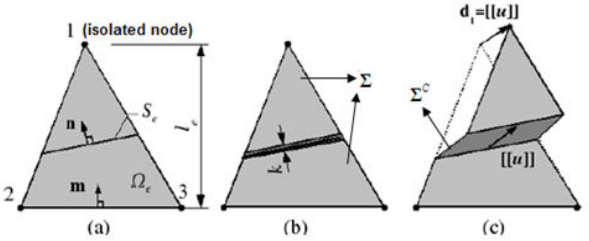

Figure 1: Element with embedded localization band [2]

3 RESULTS

The plastic rotation capacity of RC beams is analyzed with the purpose of reproducing the experimental tests reported by [3].

It was decided to begin by numerically simulating the experimental tests developed with beam B1, of length L=2000 mm, height h=200 mm and width b=100 mm, reinforced with 6-mm-diameter stirrups, with 150 mm spacing. The longitudinal tensile, ρ_t, and compression reinforcement ratio, ρ_c, is 0.57% and 0.25% for the first test, 1.13% and 0.50% for the second test, and 1,71% for the third test, respectively. Table 1 presents the mechanical and geometrical parameters for beams B1, B2 and B3. A numerical analysis was then made of the experimental tests of beams B2 and B3 (see Table 1). Figure 2 illustrates the geometric model and scheme of the tests, which, for reasons of symmetry, only had one half modeled.

Figure 3 shows the finite element mesh, the distribution of the steel bars and stirrups, and the boundary conditions for the numerical model of the beam. The concrete is represented by triangular finite elements of three nodes, while the rebars are represented by linear elements of two nodes connected to the nodes of the solid elements. To obtain the structural curve (moment-rotation), the loading process was performed by controlling the vertical displacement of the loading point located in the central section (see Fig. 3).

Table 1: Mechanical and geometric parameters

Beams	h (mm)	b (mm)	L (mm)	ρ_t (%)	ρ_c (%)	stirrups
B1	200	100	2000	0,57	0,25	ø6/150
				1,13	0,50	ø6/150
				1,71	0,50	ø6/150
B2	400	200	4000	0,28	0,20	ø6/200
				0,57	0,20	ø6/200
				1,13	0,20	ø6/200
				1,71	0,20	ø6/200
B3	600	300	6000	0,13	0,12	ø6/150
				0,25	0,12	ø6/150
				0,57	0,12	ø6/150
				1,13	0,12	ø6/150

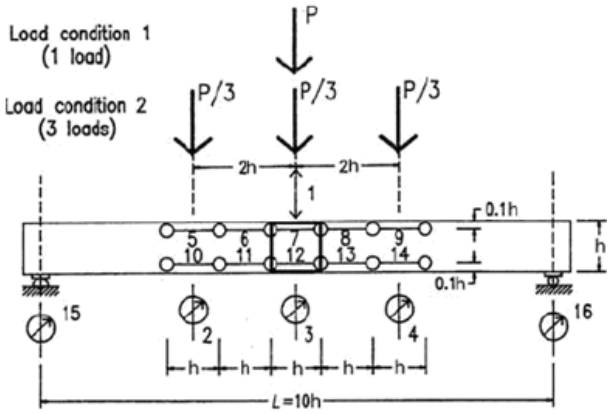

Figure 2: Geometric model of the beam [3]

The composite damage model was used to represent the nonlinear behavior of the concrete. The hardening/softening module $H = -0{,}01$ was used for the compression model, $B = 1{,}0$, and the exponential softening parameter of the tensile model $\boldsymbol{A} = 0{,}025$. The properties of the material used were: elastic modulus $\boldsymbol{E} = 34{,}690\ \boldsymbol{GPa}$, Poisson's coefficient $n = 0{,}2$, tensile strength $s_t = 2{,}66\ \boldsymbol{MPa}$ and compressive strength $s_c = 26{,}60\ \boldsymbol{MPa}$.

An elastic-perfectly plastic behavior was assumed for the steel. The properties of the material were: modulus $\boldsymbol{E} = 200{,}0\ \boldsymbol{GPa}$, Poisson's coefficient $n = 0{,}2$, and yield strength $s_y = 562{,}0\ \boldsymbol{MPa}$.

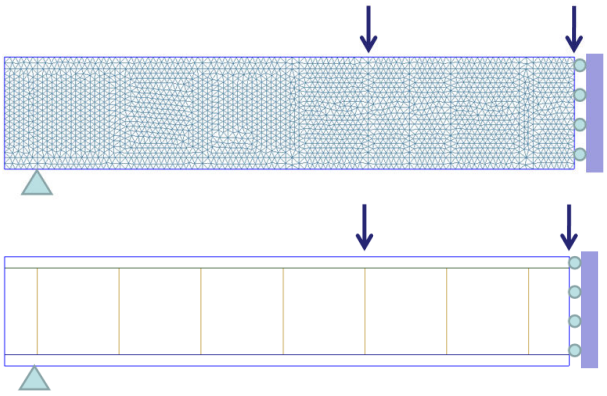

Figure 3: Finite element mesh, geometric distribution of the steel bars and stirrups, and boundary conditions of the beam

The crack pattern of beam B1-1.13 (beam B1 with longitudinal reinforcement ratio of 1.13%) obtained numerically is depicted in Figure 4, which shows the lines of embedded cracks and an overview of the variable of tensile damage.

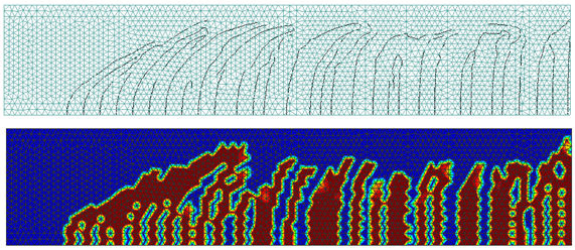

Figure 4: Crack pattern shown by lines of embedded cracks and by the tensile damage variable of beam B1-1.13

Figure 5 shows the moment vs. rotation curves for the different reinforcement ratios. Note that the numerical results reproduce well the experimental behavior characterized by a reduction in ductility in response to increasing longitudinal reinforcement.

An important factor in modeling is the ability to represent the crushing failure of concrete, which in fact defines the maximum rotation that can be achieved after ultimate yield strength of the tension reinforcement is reached. Figure 6 shows the compressive damage at the end of the analysis of the beam, when the compressed region undergoes crushing failure, which is characterized by a wedge slip mechanism delimited by shear bands. Figure 7 illustrates the different phases of the structural behavior.

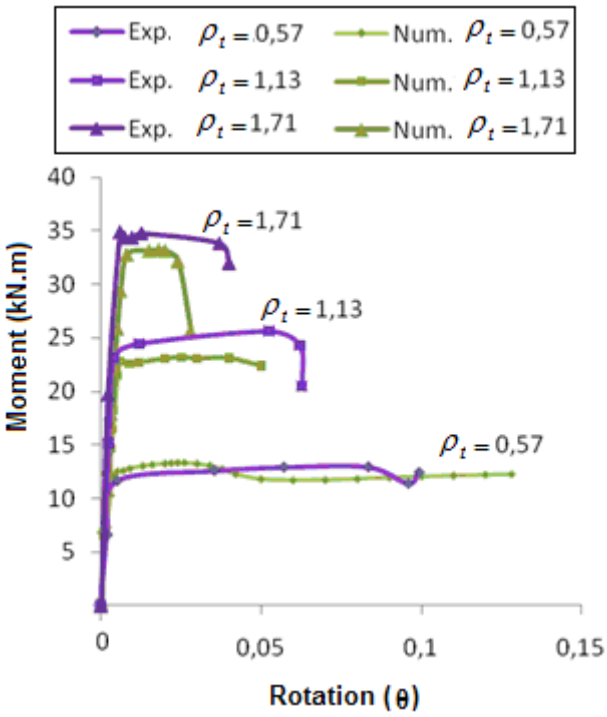

Figure 5: Moment vs. rotation curve, comparing the structural responses obtained numerically and experimentally

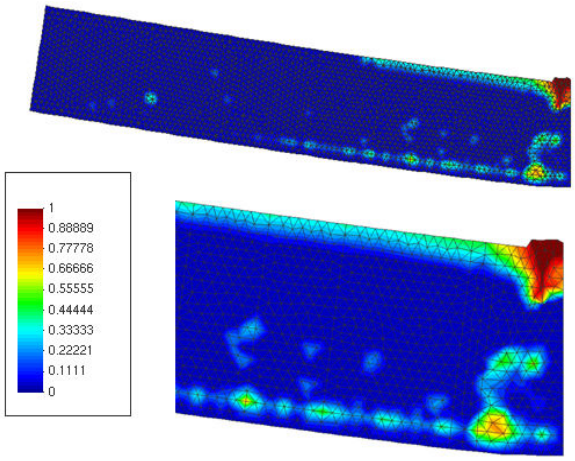

Figure 6: Crushing of the concrete due to compression in the beam (compressive damage variable)

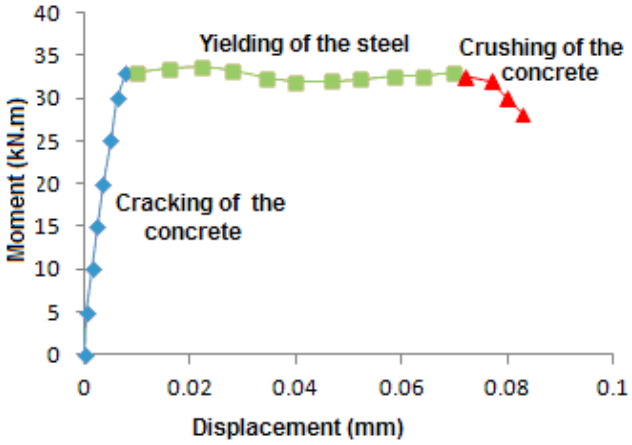

Figure 7: Phases of the structural behavior (B1, $\rho_t = 1{,}71$)

Figures 8 and 9 show the structural responses of moment vs. rotation of the tests developed with beams B2 and B3 with different reinforcement ratios (see Table 1). In general, the numerical results efficiently simulated the experimental tests developed by [3]. Varying the reinforcement ratio for beams B2 and B3 produced results similar to those of beam B1, since increasing the tension ratios led to a considerable increase in strength and a decrease in ductility. Therefore, it was found that increasing the dimensions of the beam led to a significant increase in strength but a loss in ductility (Fig. 10).

Thus, over-reinforced or oversized beams gain in strength, but with a loss in ductility, caused by crushing failure of the concrete in the compressed region, even before the tensioned steel begins to yield.

Lastly, the results of the experimental investigation carried out by [3] clearly indicate the size-scale effect of the beam in ductility after reaching the elastic limit, presenting a gain in strength and a loss in ductility in response to increasing beam dimensions. In addition, the numerical investigation demonstrated that the combined model proposed for modeling the plastic rotation capacity is able to simulate this phenomenon efficiently.

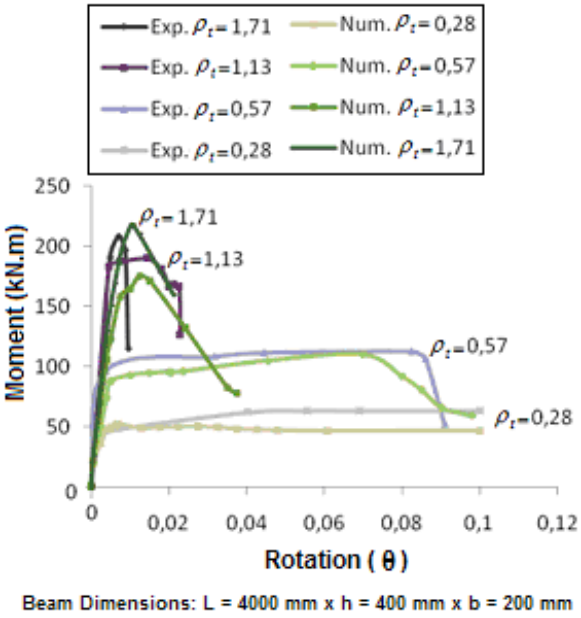

Figure 8: Moment vs. numerical and experimental rotation curve for beam B2

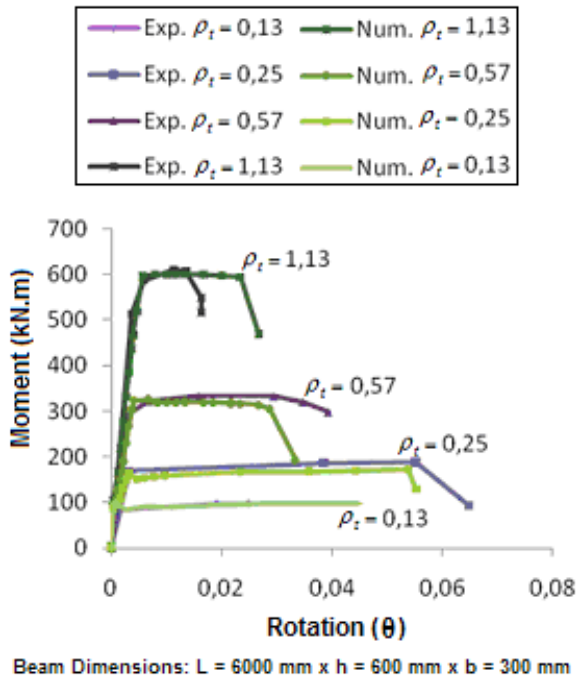

Figure 9: Moment vs. numerical and experimental rotation curve for beam B3

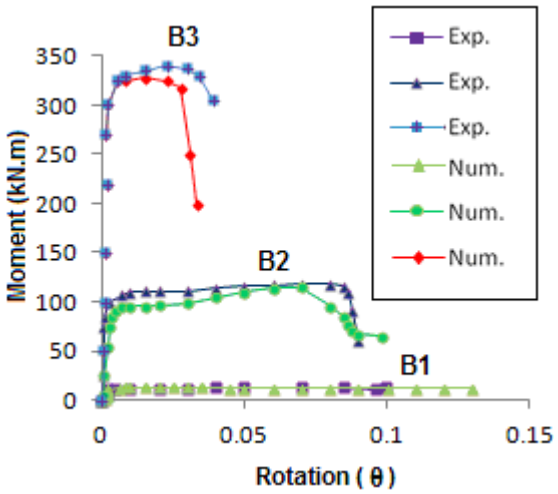

Figure 10: Moment vs. numerical and experimental rotation curve for beams B1, B2 and B3, for the same tensile reinforcement ratio ($\rho_t = 0{,}57$)

4 CONCLUSIONS

In this study a numerical analysis was developed by the finite element method of plastic rotation capacity in RC beams, using a model based solely on continuum damage mechanics (combined damage model). The combined model is able to represent the structural nonlinearity resulting from the fracture process of concrete in the tensioned region, using finite elements with embedded cracks, in the context of Continuum Strong Discontinuity Approach, and the crushing failure of concrete in the compressed region, which are phenomena that normally occur in reinforced structural elements.

Both the experimental and numerical results demonstrate the importance of the effect of compression (compressed region of the beam) on the ductile capacity of the RC beam, since the structure collapses at high tension reinforcement ratios when it reaches its ultimate compressive strength (strain domain 4). For small tension reinforcement ratios (typically reinforced or under-reinforced beams corresponding to strain domains 2 and 3), the steel's yield stresses are reached when the compressive stresses in the compressed zone are still well below the compressive strength of the concrete. In such cases, the beam develops large strains before it collapses.

5 ACKNOWLEDGMENTS

The first author gratefully acknowledges CAPES (Brazil's Federal Agency for the Support and Improvement of Higher Education) for a doctoral grant; the second author acknowledges the support of FUNDUNESP (Foundation for the Development of UNESP); and the third, fourth and fifth authors acknowledge FAPESP (São Paulo Research Foundation) for granting a doctoral and a postdoctoral fellowship.

6 REFERENCES

[1] Manzoli, O.L., Rodrigues, E. A. and Gamino, A. L., 2010. Simulação do comportamento não linear de materiais quase-frágeis via elementos finitos com fissura embebida. *Revista Internacional de Métodos Numéricos para Cálculo y Diseño en Ingeniería* **27**: 117-128.

[2] Manzoli, O.L. and Shing, B., 2006. A general technique to embed non-uniform discontinuities into standard solid finite elements. *Computers and Structures* **85**:742-757.

[3] Bosco C. and Debernardi P. G., 1992. Experimental investigation on the ultimate rotational capacity of R.C. beams. Report no. 36, Atti del Dipartimento, Politecnico di Torino, *Ingegneria Strutturale*.

[4] Carpinteri, A., Corrado, M., Mancini, G. and Paggi, M., 2009. A numerical approach to modelling size effects on the flexural ductility of RC beams. *Materials and Structures* **42**:1353-1367.

[5] Carpinteri, A., Corrado, M., 2010. Dimensional analysis approach to the plastic rotation capacity of over-reinforced concrete beams. *Engineering Fracture Mechanics* **77**:1091-1100.

[6] Lemaitre, J., Chaboche, J.L., 1985. Mechanics of solid materials. Cambridge: *University Press*.

[7] Lemaitre, J., 1992. A course on damage mechanics. *Springer-Verlag*.

[8] Oliver, J., 1996. Modeling strong discontinuities in solid mechanics via strain softening constitutive equations. part 1: Fundamentals. *Int. J. Num. Meth. Eng*. **39**(21):3575-3600.

[9] Oliver, J., 1996. Modeling strong discontinuities in solid mechanics via strain softening constitutive equations. part 1: Fundamentals. part 2: Numerical Simulation. *Int. J. Num. Meth. Eng*. **39**(21):3575-3600.

[10] Oliver, J., 1996. Modeling strong discontinuities in solid mechanics via strain softening constitutive equations. part 2: Numerical Simulation. *Int. J. Num. Meth. Eng*. **39**(21):3601-3623, 1996.

[11] Oliver, J., Cervera, M. and Manzoli, O., 1999. Strong discontinuities and continuum plasticity model: the strong. discontinuity approach. *international journal of plasticity* **15**: 319-351.

[12] Oliver, J.,2000. On the discrete constitutive models induced by strong discontinuity kinematics and continuum constitutive equations. *Int. J. Solid Struct.* **37**: 7207–7229.

[13] Oliver, J., Linero, D., Huespe, A. and Manzoli, O.L., 2008. "Two dimensional modeling of material failure in reinforced concrete by means of a continuum strong discontinuity approach. *Comput. Methods Appl. Mech. Eng.* **197**: 332-348.

[14] Manzoli, O. L., Oliver, J., Huespe, A. E. and Diaz, G., 2008. A mixture theory based method for three dimensional modeling of reinforced concrete members with embedded crack finite elements. *Computers & Concrete – An International Journal* **5**(4): 401-416.

[15] Simo, J.C. and Ju, J.W., 1987. Strain- and stress-based continuum damage models – I. Formulation, *Int. J. Solids Structures* 23: 821-840.

[16] Cervera, M., Oliver, J. and Manzoli, O., 1996. A rate-dependent isotropic damage model for the seismic analysis of concrete dams. *Earthquake Engineering and Structural Dynamics* **25**:987-1010.